

Multidimensional turbulence spectra -identifying properties of turbulent structures

Farideh Ghasempour^{1*}, Ronnie Andersson¹, Nicholas Kevlahan² and Bengt Andersson¹

¹Department of Chemical and Biological Engineering, Chemical Reaction Engineering, Chalmers University of Technology, SE-41296 Gothenburg Sweden

²Department of Mathematics and Statistics, McMaster University, Hamilton L8S 4K1, Canada

* E-mail: farideh@chalmers.se

Abstract. Development of models for several phenomena occurring in turbulent single and multiphase flows requires improved description and quantification of the turbulent structures. This is needed since often the phenomena are very fast or nonlinear. Previously the authors have presented experimental measurements that show that the breakup of bubbles and drops in turbulence is due to interaction with single turbulent vortices. Hence, it is not sufficient to use average turbulence properties when developing models for CFD simulation of engineering applications. In this paper the results from analysis of individual turbulent structures are presented. Results from analysis of the turbulent kinetic energy in turbulent structures, using Eulerian vortex identification methods, are presented. The amount of turbulent kinetic energy associated with a coherent vortex defined using different vortex identification methods is quantified. It is shown that the peak turbulent kinetic energy is located near the edge of the region identified as coherent, making the analysis challenging and development of models difficult. However, detailed analysis of a small number of coherent vortices from LES of turbulent pipe flow reveals new information about their life history. The growth (i.e. entrainment of the surrounding liquid), enstrophy, lifetime, and energy of a specific coherent vortex are tracked over time.

1. Introduction

Many important processes in turbulent flows are either very fast or strongly nonlinear e.g. bubble and drop break up, coalescence and mixing of species combined with fast chemical reactions. In modeling these phenomena it is not sufficient to use average turbulence properties (Luo and Svendsen, 1996, Andersson et al., 2004). It has been shown that fluid particles (i.e. bubbles and drops) break up within a few milliseconds due to interaction with single turbulent vortices (Andersson and Andersson, 2006b). Hence, these phenomena must be described as an interaction between fluid particles and individual turbulent structures. They should not be seen as interaction with the statistical averaged properties of turbulent structures. Among others it is necessary to know the lifetimes, number density and the distribution of turbulent kinetic energy (TKE) of vortices of various sizes (Andersson and Andersson, 2006a). Breakup of fluid particles is to a large extent determined by turbulent vortices of the same size as the fluid particles.

The turbulent vortices must exert sufficient stress to stretch the fluid particle and also transfer sufficient energy to increase the interfacial area (Andersson and Andersson, 2006b). Hence, simulation of turbulent dispersions requires closure models in the population balance equations for the break-up of bubbles and drops, e.g. models for the vortex energy. Quantitative prediction of the breakup rate requires detailed information of the disruptive turbulent stresses. These calculations are done using basic models for the average vortex energy and distribution of energy for all vortex sizes within the

energy cascade. The average vortex energy, in the inertial subrange, for an vortex of size λ is (Luo and Svendsen, 1996, Hagesaether et al., 2002, Andersson and Andersson, 2006a)

$$\bar{e}(\lambda) = \rho_c \frac{\pi \lambda^3}{6} \frac{\bar{u}_\lambda^2}{2}. \quad (1)$$

It is often assumed that for each λ there is a distribution of fluctuating velocities and the normalized energy distribution is given by (Angelidou et al., 1979, Luo and Svendsen, 1996)

$$\varphi(\chi) = \exp(-\chi) \quad (2)$$

where $\chi = e(\lambda)/\bar{e}(\lambda)$ which defines the ratio of the vortex energy to the average vortex energy.

One important mechanism for coalescence is the trapping of two or more fluid particles in a turbulent vortex with higher density than the particles. The vortex must be large enough to capture the particles and have sufficient vorticity and life span for the particles to move together and drain the liquid film between the two flattening interfaces.

Turbulent mixing is occurs via the entrainment of a second species into a growing turbulent vortex and the stretching of the vortex. This stretching makes the mixing layers thinner and thus enhance the mixing rate through decreased diffusion length and time scales. Hence, knowledge of liquid entrainment and stretching is also needed in the case of turbulent mixing combined with chemical reactions where the rate of reactant entrainment and stretching of the turbulent vortices determines the local concentrations and consequently the selectivity of the reactions (Bouaifi et al., 2004).

The purpose of the present work is to develop and evaluate tools to identify and track individual coherent vortices over their whole lifetimes. This allows individual vortices to be visualized and their turbulent properties to be measured over time as they interact with other flow structures. Over the last two decades much work has been done to develop visualization methods, but little progress has been made in extracting and quantifying the data needed in model development. Accurately tracking individual coherent vortices is necessary in order to understand the role turbulent structures play in mixing and other processes. Indeed, the term 'coherent' suggests that the definition of a coherent vortex must include time information.

2. Vortex identification methods

Visualization of vortices has been investigated for two-and three-dimensional turbulence over the last two decades. Ideally, the visualization of the turbulent vortices should give their sizes, locations, velocities and allow quantification of turbulent properties such as kinetic energy, vorticity, vortex volume as a function of time. Several methods for identifying vortices have been proposed, but little work has been done to quantify these dynamical properties. They have been classified as either Eulerian or Lagrangian methods.

Eulerian methods for identifying flow structures are generally formulated in terms of the invariants of the velocity gradient tensor $\nabla \mathbf{u}$. These criteria can be the iso-surfaces of vorticity, second invariant of $\nabla \mathbf{u}$, complex eigenvalues of velocity gradient tensor, λ_2 and pressure minimum. Local pressure minima has also be used to identify vortices. Since swirling motion is not always associated with a sectional pressure minimum, this method alone is not useful for identifying vortices (Jeong and Hussain, 1995, Kida and Miura, 1998). Kida (1998) applied the sectional swirl and pressure minimum scheme and vortex skeleton and applied it to identify coherent vortices in homogenous turbulence. The vortex skeleton was constructed by tracing the lines of sectional swirl pressure minimum and the vortical regions surrounding them outlined.

Relying on iso-surfaces of vorticity magnitude makes recognizing swirling and shearing motions problematic (Tanaka and Kida, 1993, Kida and Miura, 1998). Many authors have suggested other methods to identify the turbulent vortices but there is no generally accepted method.

The second invariant of $\nabla \mathbf{u}$ (or the Q criterion) represents the local balance between rotation rate and strain rate (Hunt, 1987).

$$Q = \frac{1}{2} \left(|\boldsymbol{\Omega}|^2 - |\mathbf{S}|^2 \right) \quad (3)$$

Here $\boldsymbol{\Omega}$ and \mathbf{S} are respectively the antisymmetric and symmetric components of $\nabla \mathbf{u}$. Regions where $Q > 0$ (with the additional condition that the pressure should be lower than the ambient pressure), are

defined as coherent vortices. Tabor (1994) proposed to account for the net rotation in the average flow, which modified the Q criterion in the following way.

$$Q_s = \frac{1}{2} \left(|\boldsymbol{\Omega} - \boldsymbol{\Omega}_s|^2 - |\mathbf{S}|^2 \right) > 0 \quad (4)$$

Where $\boldsymbol{\Omega}_s$ is a matrix, containing derivatives of the steady rotation rate.

Applying the Q criterion is not appropriate when the vortex expands locally due to an imposed non-uniform strain field (Jeong and Hussain, 1995). Adding a measure of the spiraling compactness of the fluid particle orbits in the vortices has also been proposed to identify the vortex cores (Chakraborty et al., 2005). This removes the drawback of the Q criterion that it cannot identify vortices in non-uniform strain.

Chong (1990) has used eigenvalue analysis of the velocity gradient tensor, $\nabla \mathbf{u}$, to identify local stream line patterns around any point in the flow in a reference frame moving with the velocity of that point. They proposed a criterion that a vortex exists when the discriminant (Δ) is positive.

$$\Delta = \left(\frac{Q}{3} \right)^3 + \left(\frac{\det \nabla \mathbf{u}}{2} \right)^2 \quad (5)$$

Kida (1998) has also used this criterion, $\Delta > 0$, for analysis of vortices in homogenous turbulence.

Jeong (1995) used the second largest eigenvalues, λ_2 , of $\boldsymbol{\Omega}^2 + \mathbf{S}^2$ and identified vortices as regions where λ_2 is negative.

McWilliams (1990) traced the boundaries of two-dimensional vortices in space and Doglioli (2007) followed the vortices in time. A similar approach to track coherent vortices in space and time is developed in this work and applied to large vortex simulation data of pipe flow.

In contrast to the above Eulerian methods, the Lagrangian methods define flow structures based on fluid particle trajectories. They identify more details of structure boundaries without relying on a pre-defined threshold. However, they are significantly more expensive computationally (Green et al., 2007). Biferale (2010) have studied vortex filament lifetime statistics in turbulence by following the trapping events of massless tracer particles inside a vortex filament.

3. Vortex tracking method

In this work we have developed an algorithm based on a combination of the McWilliams and Doglioli methods (McWilliams, 1990, Doglioli et al., 2007). This tool helps to select and follow a single turbulent vortex in the tangle of vortex filaments found in the flow domain. More specifically, the algorithm is an extension of the approach of McWilliams from two dimensions to three dimensions, while the vortices are tracked in time using Doglioli's approach. Using this tool it is possible to track the shape and other properties of the selected vortex over time. It allows several properties to be quantified within a coherent vortex such as its volume, aspect ratio, center of mass, enstrophy, turbulent kinetic energy, etc. The tracking procedure can be decomposed into the following three steps:

3.1. Vortex cross-section and boundary region tracking

As mentioned in previous section, since there is no imposed non-uniform strain field in our example flow, the Q criterion has been used to identify the location of the turbulent vortex. The vorticity and the Q criterion are large at the walls and thus Q and vorticity are normalized in order to identify turbulent structures in the bulk of the flow, as discussed in the results section. In this work, the following normalization of the Q criterion was used

$$Q_n = \frac{Q}{0.5 |\boldsymbol{\Omega}|^2} \quad (6)$$

This choice of normalization allows more turbulent structures to be identified in the flow (not just the strongest ones). A local normalization with vorticity makes large (but weaker) vortices in the bulk flow easier to identify, as shown in the results section.

At a specific time all vortices in a two-dimensional plane identified by a specified iso- Q_n threshold were visualized and one of these vortices was selected for tracking. Two points on the boundary of the selected vortex were identified and, starting from the first boundary point, the vortex surface was traced along parallel grid lines for specified threshold values until reaching the second boundary point. This defines the closed boundary curve of the vortex in a particular plane. The vortex cross section, S , is defined by the all points included inside the boundary curve. Different threshold values for iso- Q_n were considered and we selected 0.1 as providing a good balance that captures the core of the vortex, but leaves out most of the incoherent vorticity.

3.2. Vortex volume tracking

For the selected vortex, step 3.1 is repeated on adjacent parallel planes to find the shape in the third dimension. The iso- Q_n volume that belongs to the same vortex, V , is constructed by joining nearby vortex cross sections, S , to define the bounding surface of the three-dimensional vortex (see equation (7)).

3.3. Time tracking

Finally, for each iso- Q_n volume identified as a vortex in the previous steps, steps 3.1 and 3.2 are repeated for a sequence of times. This tracking is performed both forward and backward in time in order to find the birth and death times of the selected vortex and to quantify the changes in its flow properties during its whole lifetime. For each selected vortex the volume, enstrophy, turbulent kinetic energy, center of mass and aspect ratio are computed. At a given time, the volume taken up by each vortex can be calculated as:

$$V = \sum_{i=1}^k S_i \cdot \Delta x \quad \& \quad S = N \cdot s' \quad (7)$$

In this equation, N is the number of cells in each cross section, s' is the surface of each cell and Δx is the distance between planes. It should be noted that the mesh is completely hexahedral and equal size in dimensions. Enstrophy is found by summing the square of the vorticity over the vortex volume. The enstrophy gradient helps to determine if the vortex is being stretched or compressed. Another way to determine whether the vortex is being stretched or not is to measure its aspect ratio. According to equation (8) the aspect ratio of a vortex is the ratio of its diameter and length. It is estimated from the volume and vortex length

$$\frac{L}{d} = \frac{1}{2} \sqrt{\frac{\pi L^3}{V}} \quad (8)$$

TKE is computed as the sum of turbulent kinetic energy over the vortex volume at each time. In order to understand how the vortex is moving, its center of mass is also tracked and the direction of vorticity in the identified center of mass point is calculated.

3.4 Computational details

In this study, a turbulent pipe flow ($\varnothing=5$ cm, $L=20$ cm) of water at $Re=20,000$ was simulated using dynamic large eddy simulation (LES). A structured hexahedral mesh containing 4.6 million cells was used and periodic boundary condition was applied. More than 97% of the total turbulent energy in the bulk of the flow and more than 80% at $y^+ > 5$ is resolved in the LES simulations. However below $y^+=5$ the subgrid turbulent viscosity ratio is below 0.1. The maximum subgrid turbulent viscosity ratio in the bulk of the flow is 1.55. Maximum instantaneous wall y^+ is 1.7 and average wall y^+ is 0.85.

4. Results

In this work several Eulerian vortex identification methods suggested in the literature were applied and the amount of turbulent kinetic energy captured was quantified. After selecting one vortex identification method which best satisfies the objectives of this research a few vortices were studied using the new tracking algorithm developed for this purpose. This algorithm reveals details of the life history of the vortices. The growth in time (i.e. entrainment of the surrounding liquid), enstrophy, and lifetime of the vortices is presented below.

4.1. Turbulent kinetic energy and different vortex identification methods

Analysis of the Lamb-Oseen vortex and LES data reveal how much energy the different vortex identification methods capture. Figure 1 shows the Q -criterion and the kinetic energy as a function of radius for an ideal Lamb-Oseen vortex. For the Lamb-Oseen vortex, the amount of turbulent kinetic energy identified by the Q criterion equals 27% when integrating the kinetic energy from the core center to five times the core radius. Hence most of the TKE is located near the edge of the vorticity dominated region, i.e. outside $Q > 0$.

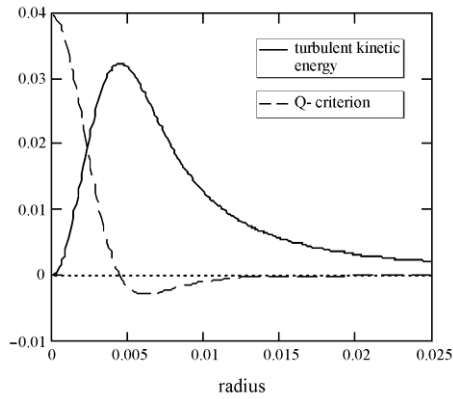


Figure 1. Turbulent kinetic energy and the coherent region identified with the Q criterion for a Lamb-Oseen vortex.

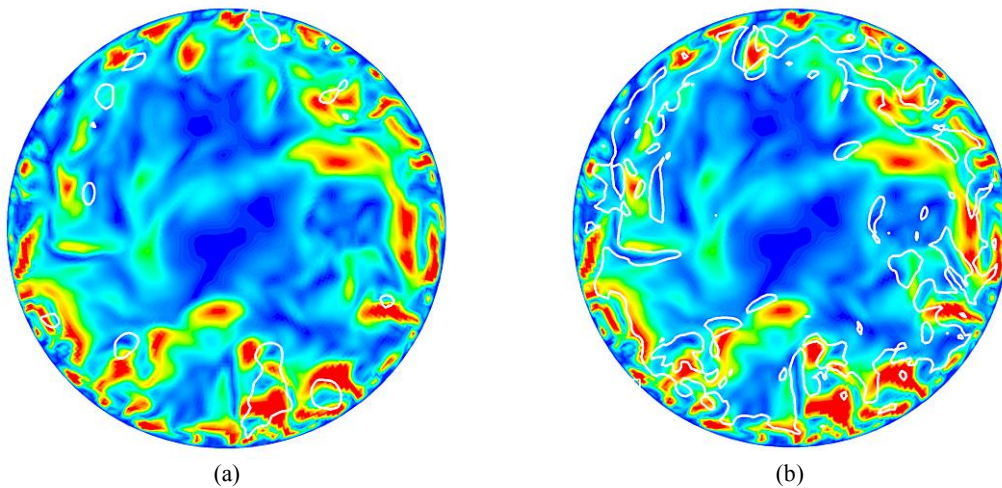


Figure 2. Overlap of turbulent kinetic energy, $0 < \text{TKE} < 0.003 \text{ [m}^2/\text{s}^2]$ and turbulent structures identified by a.) Iso-pressure = -3 [Pa] b.) Iso-vorticity magnitude = 50 [1/s].

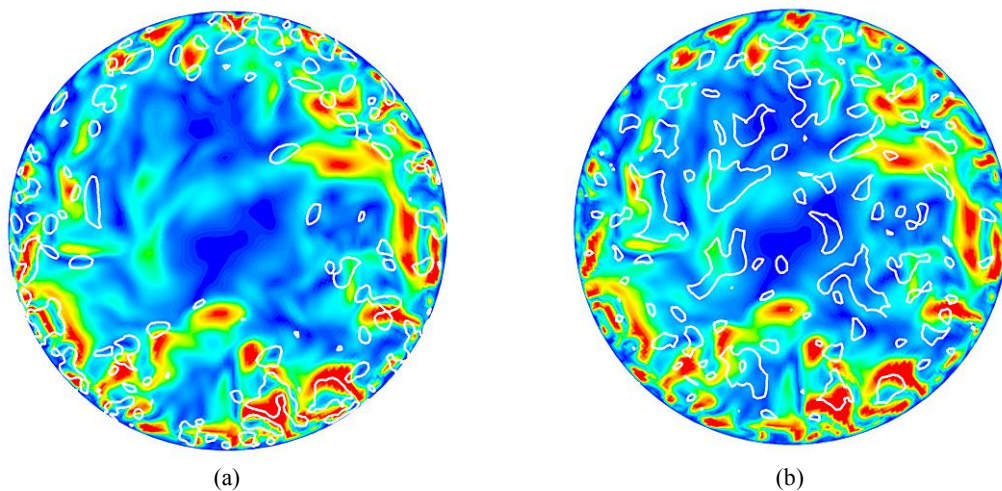


Figure 3. Overlap of turbulent kinetic energy, $0 < \text{TKE} < 0.003 \text{ [m}^2/\text{s}^2]$ and turbulent structures identified by a.) Iso- Q criterion = 1000 [1/s²], b.) Iso- Q_n criterion = 0.5 [-].

Figures 2-3 shows different means of capturing the turbulent kinetic energy in a vortex. As shown in Figure 2a few structures are identified using an iso-pressure criterion. Here the colored contour plot shows the instantaneous TKE and the white circular regions represent iso-lines of pressure. Figure 2b shows the iso-vorticity magnitude, which identifies a large part of the near wall region as coherent vortices. This over-identification problem is partly overcome by accounting for the balance between rotation and strain rates as shown in Figure 3a using the Q criterion. As can be seen in Figure 3a, there are few vortices identified in the bulk region. As seen in Figure 3b more structures in the bulk are identified using the Q_n criterion. This criterion allows structures with intermediate vorticity in the bulk to be identified more easily, see Figure 3b.

For a certain ratio of vortex surface to total cross-section the ratio of turbulent kinetic energy to the total turbulent kinetic energy in the cross-section are summarized in Table 1. This comparison is made for different vortex identification methods. Although the iso-vorticity method gives highest ratio it does not fulfill the objectives, since it cannot associate this energy with individual turbulent vortices in the near wall region. The correlation between iso-pressure zones and the turbulent kinetic energy is low. Furthermore it identifies very few vortices (see Figure 2a).

For all vortex identification methods examined, threshold values must be chosen. In Table 2 it is shown how the selection of the threshold value affects the amount of energy captured. Both Q criteria methods have similar properties and are sensitive to the choice of threshold value. Even if the threshold is decreased to a minimum positive value, no more than 50% of the turbulent kinetic energy is captured. The major drawback of reducing the threshold value to these low levels is that the boundaries of the coherent structures merge with each other and we include non-coherent vorticity.

It is important to note that even if most TKE is not contained within the bounding surface of the vortex, the entire TKE associated with the vortex can always be found by calculating the velocity generated by the vortex core using the Biot-Savart law. Thus, since vorticity is much more localized than velocity, we do not expect that an accurate vortex identification method should necessarily capture all (or even most) of the TKE associated with the vortex within the identified vortex volume.

Table 1. Turbulent properties quantified with different vortex identification methods.

	Iso-pressure	Iso-vorticity magnitude	Q criterion	Q normalized (Q_n)
TKE/TKE total [%]	25.6	48.8	36.7	32.6
Vortex surface/total surface [%]	34.6	34.8	34.7	34.7

Table 2. Turbulent properties as a function of the Q criterion threshold value.

	Q criterion [$1/s^2$]			Q_n criterion		
	100	70	50	0.15	0.1	0.05
TKE/TKEtotal [%]	36.7	38.90	40.6	29.2	32.6	36.5
Vortex surface/total surface [%]	34.7	37.54	39.6	31.8	34.7	37.9

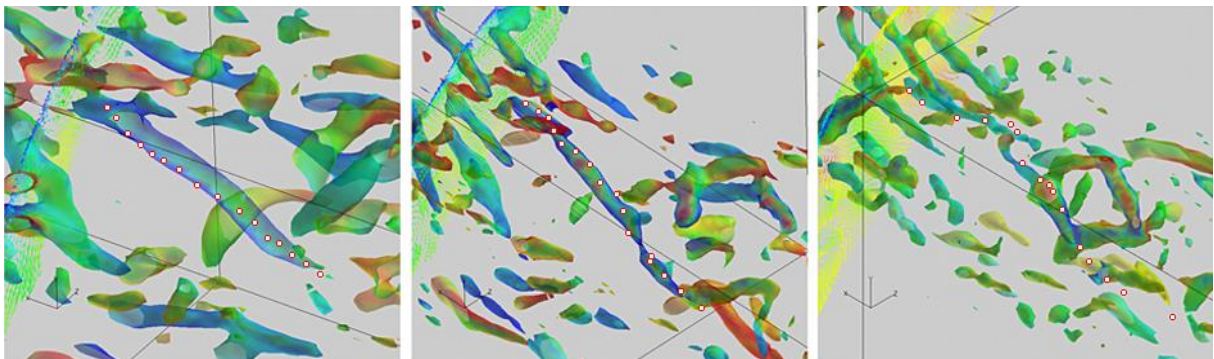


Figure 4. Time sequence of turbulent vortex with Lagrangian particle tracking at 24 ms, 52 ms and 93.5 ms after injection time.

Tracking vortices with particles gives important additional dynamical information. Sixteen particles were injected uniformly in a single vortex. Figure 4 shows the vortex and the particles at 24, 52 and 93.5 ms after injection. The vortex identified by the Q criterion moves faster than the fluid particles in the vortex. As seen, after 24 ms there are no particles remain in the front part of the vortex and some particles have been left behind. One small part of the vortex is almost detached from the larger part at 52 ms, and at 93.5 ms only fragments of the original vortex remain.

4.2. Vortex properties

In this study, three different vortices were selected, identified and isolated using the algorithm described in the previous section. Several characteristic properties of these vortices were quantified. These vortices were located at $y^+ = 160, 100$ and 50 respectively. Figure 5 shows a turbulent vortex from birth to death. The contour shows the iso- Q_n surface for $Q_n = 0.1$. The figure shows a single turbulent vortex that is mainly aligned with axial flow. It has an irregular shape since stretching, bending, local shear rate and the surrounding vortices will affect the local Q -value.

The first vortex is selected at $y^+ = 160$, which corresponds to a location approximately 1/3 of the radius from the wall. The selected vortex was followed backward and forward in time to find the birth and death points. This was done by applying the algorithm starting at time 6.5001 s, as shown in the upper right corner of Figure 5. Figure 5 shows that the vortex was formed by the merger of two small vortices with the same rotation direction. The merged vortex (centre of mass) slowly migrates toward the wall for 20 ms, and then moves back in to the bulk region. It can be seen that for the rest of its life time it moves toward the bulk region. As shown in Figure 6a, the volume of this vortex varies in time: first increasing, reaching a maximum and then decreasing. It should be noted that in Figure 6a the initial volume of first vortex was calculated as the sum of the two small parent vortices. During its 160 ms lifetime this vortex is rotating, stretching, bending and finally splits into two different rotation direction vortices. After splitting, the volumes of the two parts decrease. Moreover, the amount of TKE captured within the threshold $Q_n > 0.1$ changes in time. It can be seen in Figure 7b, that the final dissipation of the vortex is followed by a rapid decrease in TKE.

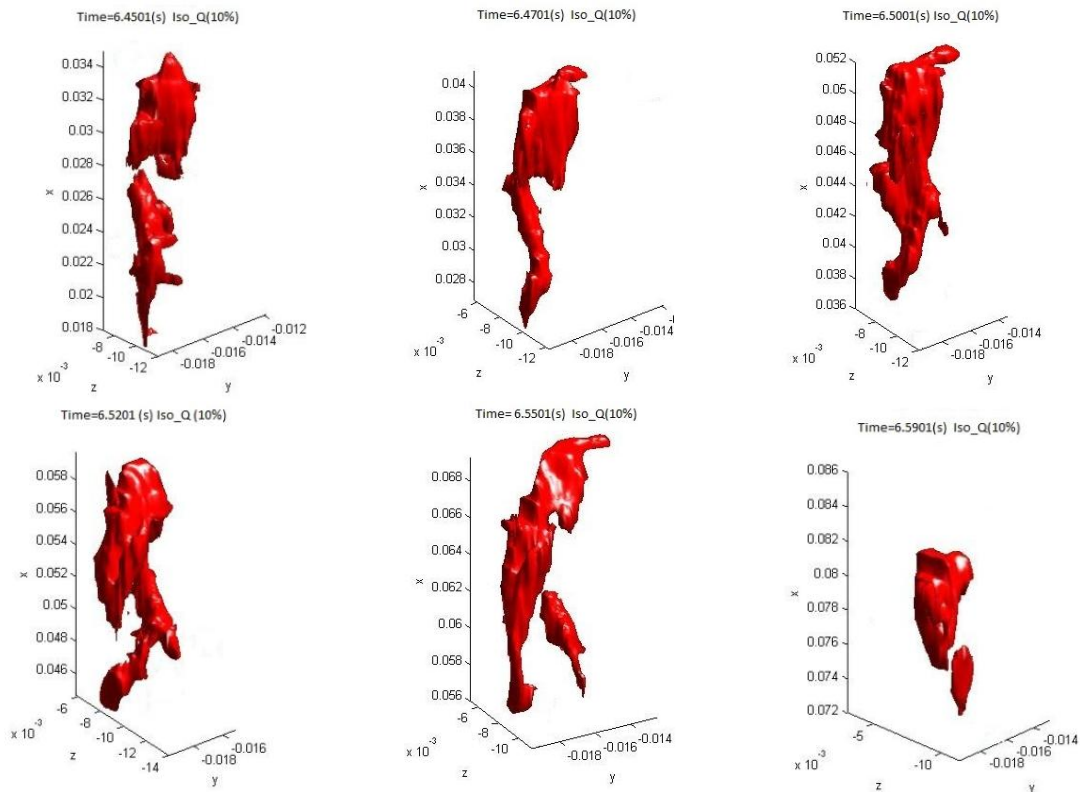


Figure 5. Time sequence of 1st turbulent vortex- birth/stretching/breakup.

The second vortex identified at around $y^+ = 100$ grows from an initially small volume. On average this vortex moves towards the bulk. However after 110 ms it migrates back towards the wall. After 120 ms it breaks into two parts, and the larger fraction has been stretched again. It should be mentioned that the last increase in volume shown in Figure 6a for the second vortex occurs at the same time as it captures additional TKE. According to Figure 7b, the new fragment of the vortex captures a large amount of TKE during the final stretching. Larger fluctuations of the center of mass for this vortex, compared to the first vortex, are also observed. This is reasonable due to its location closer to the wall. This vortex is capturing TKE in the beginning and then it decreases up to the breakage point. However, after the breakage, as mentioned above, the amount of TKE increases again.

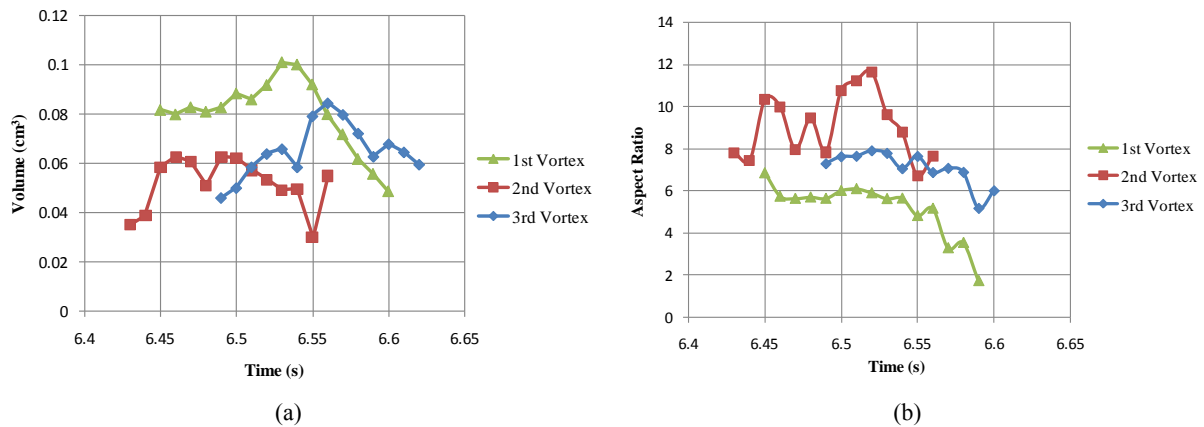


Figure 6. a.) Growth of turbulent vortices b.) vortex aspect ratio

The third selected vortex was located at $y^+ = 50$. This vortex is also growing in volume and capturing TKE as it moves in both y and z directions toward the bulk region. During 120 ms it can be seen that its volume is initially growing rapidly, while its aspect ratio (seen in Figure 6b) is almost constant. Thus, the vortex is growing in both length and diameter. For vortices one and three there is a simultaneous peak in volume and TKE (as expected), while for vortex number two it is not that clear, although the correlation is still high.

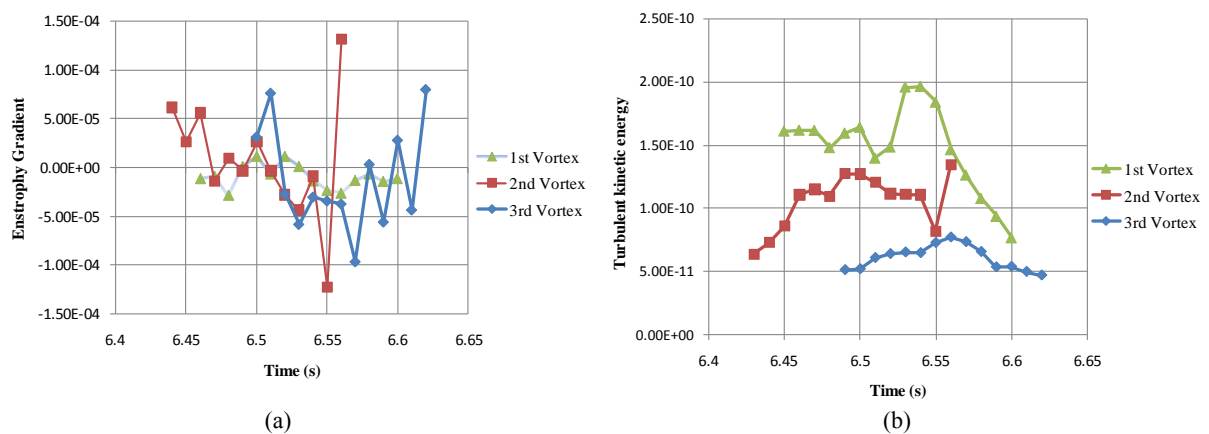


Figure 7. a.) Enstrophy gradient b.) TKE

5. Discussion and Conclusions

The objective of this study was to quantify turbulent properties that are fundamental for many phenomena in chemical engineering e.g. the mixing of species and breakup and the coalescence of fluid particles. Too few vortices have been studied to be able to make general conclusions, or calculate statistics, about the dynamics of individual turbulence vortices. However, some general conclusions about the evaluation tools can be made. Although one must be cautious in drawing conclusions about

multiphase flow from these simulations of single phase flow, the observations should be valid for multiphase flow at low volume fraction of dispersed phase.

Different criteria for identifying a vortex structure found different structures. Only the very large turbulent vortices with high vorticity were identified by all methods. The shape and the exact locations of these vortices were not the same, but they all gave similar qualitative identifications of vortex structures. The pressure criterion was the most difficult to apply as it was very sensitive to the pressure threshold. Iso-vorticity was also sensitive to the threshold level.

The Q criterion and the normalized Q_n criterion were found to be the most stable criteria: a change in threshold of the criterion did not change the structure very much. Of course, our choice of normalization revealed more of the large turbulent vortices in the bulk of the flow and, depending on the selected threshold, it will affect identification of turbulent structures in the near wall region.

The Eulerian approach to identify turbulent structures does not reveal the whole picture. Lagrangian simulations of tracer particles that follow the fluid elements show that the behavior of the turbulent vortices is more complex and dynamic. The fluid particles in the turbulent vortices may not be the same during the whole life span of the vortex. Some fluid particles may be lost and new fluid elements included as the vortex evolves. The Eulerian evaluation follows the structure while the Lagrangian follow the fluid elements. In our chemical engineering applications, this distinction is important.

The concept of the 'lifetime' of a turbulent vortex turned out to be complex and difficult to define objectively. The simple birth point of a turbulent vortex, as suggested by Hunt and Morrison (2000) for an idealized flow was not observed for all vortices. There is also a continuous break-up and merging of turbulent vortices at the walls. Some of these vortices are dissipated while others gain energy and grow in size. In our analysis we have used the rapid growth observed initially to identify 'birth'. This fast increase in size may be due both to the merger of distinct vortices and to the growth of single vortices. In contrast, the 'death' of a vortex is more easily observed, even though the vortices typically break up into several fragments. The resulting very small vortices then dissipate very quickly.

Due to the fact that vorticity is much more localized than velocity, most of the turbulent kinetic energy is necessarily located outside the volume defined by the iso- Q_n value. However, if the Lamb-Oseen vortex is a reasonable approximation of a turbulent vortex, this fraction should be fairly constant. This requires that most of the turbulent kinetic energy is located in the vicinity of the observed turbulent structures. If necessary, the entire velocity field associated with an identified vortex could be recovered using the Biot-Savart equation. This hypothesis is reasonable, but must be tested further using actual turbulence data.

The proposal to use the integrated turbulent energy to evaluate whether individual vortices have sufficient energy to break a bubble or drop must be re-examined in the light of the current results. The very large aspect ratios we found, even for turbulent vortices in the bulk, suggests that it is unlikely that the whole vortex interacts with bubbles and drops. Even including the surrounding turbulent kinetic energy, and extending the vortex radius, the aspect ratio will be in the range 3-5.

The coalescence of fluid particles due to trapping and movement of particles towards the center of the vortex is mostly affected by the size of the vortex, its vorticity and its lifetime. All these properties can be obtained using the vortex tracking algorithm developed here. The local characteristics of the turbulent structures in the vicinity a single fluid particle could affect the turbulent properties. However, for a very dilute system we expect that the results are valid.

Mixing of two species is to a large extent determined by entrainment of the second component into a turbulent vortex. Growth of a turbulent vortex, defined as the increase in volume within the iso- Q_n criterion, was observed easily. Entrainment of fluid while shedding other parts of the vortex was also observed. Full description of mixing requires additional information that could be obtained using Lagrangian particle tracking. Increasing mixing rate by stretching a turbulent vortex might be signalled by an increase in enstrophy or aspect ratio. Change in aspect ratio or enstrophy are correlated, but the correlation is not very high. This could be due to shedding of parts of the vortex. Thus, it should be more appropriate to correlate mixing rate with enstrophy.

6. References

- ANDERSSON, R. & ANDERSSON, B. 2006a. Modeling the breakup of fluid particles in turbulent flows. *AIChE Journal*, **52**, 2031-2038.
- ANDERSSON, R. & ANDERSSON, B. 2006b. On the breakup of fluid particles in turbulent flows. *AIChE Journal*, **52**, 2020-2030.
- ANDERSSON, R., ANDERSSON, B., CHOPARD, F. & NOREN, T. 2004. Development of a multi-scale simulation method for design of novel multiphase reactors. *Chemical Engineering Science*, **59**, 4911-4917.
- ANGELIDOU, C., PSIMOPOULOS, M. & JAMESON, G. J. 1979. Size distribution functions of dispersions. *Chemical Engineering Science*, **34**, 671-676.
- BIFERALE, L., SCAGLIARINI, A. & TOSCHI, F. 2010. On the measurement of vortex filament lifetime statistics in turbulence. *Physics of fluids*, **22**.
- BOUAIFI, M., MORTENSEN, M., ANDERSSON, R., ORCIUCH, W. & ANDERSSON, B. 2004. Experimental and numerical investigations of jet mixing in a multifunctional channel reactor: Passive and reactive systems. *Chemical Engineering Research and Design*, **82**, 274-283.
- CHAKRABORTY, P., BALACHANDAR, S. & ADRIAN, R. J. 2005. On the relationships between local vortex identification schemes. *Journal of Fluid Mechanics*, **535**, 189-214.
- CHONG, M. S., PERRY, A. E. & CANTWELL, B. J. 1990. A general classification of 3-dimensional flow-fields. *Physics of Fluids a-Fluid Dynamics*, **2**, 765-777.
- DOGLIOLI, A. M., BLANKE, B., SPEICH, S. & LAPEYRE, G. 2007. Tracking coherent structures in a regional ocean model with wavelet analysis: Application to Cape Basin vortices. *Journal of Geophysical Research-Oceans*, **112**.
- GREEN, M. A., ROWLEY, C. W. & HALLER, G. 2007. Detection of Lagrangian coherent structures in three-dimensional turbulence. *Journal of Fluid Mechanics*, **572**, 111-120.
- HAGESAETHER, L., JAKOBSEN, H. A. & SVENDSEN, H. F. 2002. A model for turbulent binary breakup of dispersed fluid particles. *Chemical Engineering Science*, **57**, 3251-3267.
- HUNT, J. C. R. & MORRISON, J. F. 2000. Vortex structure in turbulent boundary layers. *European Journal of Mechanics B-Fluids*, **19**, 673-694.
- JEONG, J. & HUSSAIN, F. 1995. On the identification of a vortex. *Journal of Fluid Mechanics*, **285**, 69-94.
- KIDA, S. & MIURA, H. 1998. Identification and analysis of vortical structures. *European Journal of Mechanics B-Fluids*, **17**, 471-488.
- LUO, H. & SVENDSEN, H. F. 1996. Theoretical model for drop and bubble breakup in turbulent dispersions. *AIChE Journal*, **42**, 1225-1233.
- MCWILLIAMS, J. C. 1990. The vortices of 2-dimensional turbulence. *Journal of Fluid Mechanics*, **219**, 361-385.
- TABOR, M. & KLAPPER, I. 1994. Stretching and alignment in chaotic and turbulent flows. *Chaos Solitons & Fractals*, **4**, 1031-1055.
- TANAKA, M. & KIDA, S. 1993. Characterization of vortex tubes and sheets. *Physics of Fluids a-Fluid Dynamics*, **5**, 2079-2080.